Optics Letters

Improved temporal characteristics for post-compressed pulses via application-tailored nonlinear polarization ellipse rotation

Esmerando Escoto,[1,*] Federico Pressacco,[1] Yujiao Jiang,[1] Supriya Rajhans,[1,2] Nikita Khodakovskiy,[1] Ingmar Hartl,[1,3] Marcus Seidel,[1,4,5] Christoph M. Heyl,[1,4,5] and Henrik Tünnermann[1,3,6]

[1]Deutsches Elektronen-Synchrotron DESY, Notkestraße 85, Hamburg 22607, Germany
[2]Friedrich-Schiller-Universität Jena, Max-Wien-Platz 1, Jena 07743, Germany
[3]HIR^{6X}: Helmholtz International Laboratory on Reliability, Repetition, Results at the most Advanced X-Ray Sources, Germany
[4]Helmholtz Institute Jena, Fröbelstieg 3, Jena 07743, Germany
[5]GSI Helmholtzzentrum für Schwerionenforschung GmbH, Planckstraße 1, Darmstadt 64291, Germany
[6]henrik.tuennermann@desy.de
*esmerando.escoto@desy.de

Received 19 August 2024; revised 5 November 2024; accepted 5 November 2024; posted 6 November 2024; published 26 November 2024

Intense ultrashort laser pulses with high temporal quality are essential for fundamental science. Nonlinear polarization ellipse rotation (NER) is one way to ensure this high temporal quality, by suppressing weaker signals beyond the duration of the main pulse up to a few orders of magnitude. Post-compression schemes have revolutionized ultrafast lasers, enabling the generation of pulses with durations beyond the limit supported by laser gain media. However, high compression ratios lead to the formation of new pre- and post-pulses. Both NER and post-compression depend on the optical Kerr effect. This makes the combination of the two in a single setup both advantageous and straightforward. While NER cannot suppress the new pre- and post-pulses generated in post-compression, we show via simulations and experimental data that by combining the two, it is possible to shape the output spectrum and counteract temporal contrast degradation.

https://doi.org/10.1364/OL.539646

The presence of pre-pulses or a strong pedestal in a high power pulsed laser is detrimental for laser–matter interaction experiments, since the weaker parts outside of the main pulse can interact with the target and change its properties, e.g., by generating a plasma that can affect the incoming main pulse [1]. Several ideas have been proposed to avoid this problem, such as the use of plasma mirrors [2,3], saturable absorbers [4], cross-polarized wave generation (XPW) [1,5], and nonlinear polarization ellipse rotation (NER) [6]. NER can reach higher transmission efficiencies than most other pulse cleaning techniques [7]. The transmission depends on the amount of nonlinear phase shift that can be accumulated by the pulse. Using an elliptically polarized input, the nonlinear phase shift—mostly due to the optical Kerr effect—induces an intensity-dependent polarization rotation, which can be used to separate the high intensity parts of the pulse from the weaker pedestal and satellite pulses. The technique has been revisited in the past years, due to the recent advancements in post-compression especially using multi-pass cells (MPCs) [8,9]. MPCs routinely allow the achievement of high B-integrals, which define the accumulated nonlinear phase shift, while maintaining the spatial mode of the beam and ensuring a uniform profile. This allows large compression factors with high throughput [9]. The higher B-integral enables the rotation of a greater proportion of the pulse, hence making it possible to reach higher NER efficiencies using MPCs [10]. NER has now been used with MPCs for both Ti:sapphire-based [11] and Yb-based lasers [12–14]. NER and post-compression can be advantageously combined as the accumulated nonlinear phase shift can be used simultaneously for both temporal pulse cleaning and temporal compression [10,11,15,16].

A remaining key challenge for post-compressed lasers is the temporal pulse quality at time scales close to the duration of the compressed pulse, wherein pre- and post-pulses are typically generated at large compression factors (>10) [17–19]. An efficient method for temporal pulse cleaning that suppresses these pre-/post-pulses during or after post-compression is still missing. If implemented in combination with spectral broadening, NER usually does not suppress pre-/post-pulses as they only appear upon compression of the spectrally broadened pulses.

We address the challenge of temporal contrast degradation in post-compression by utilizing a new NER regime. Via advanced polarization state control, we demonstrate how the new output spectrum and thus the temporal contrast can be optimized to minimize pre-/post-pulses. First, we demonstrate how NER can be modeled accurately in an MPC and show how analytical equations can closely predict key process characteristics. We then

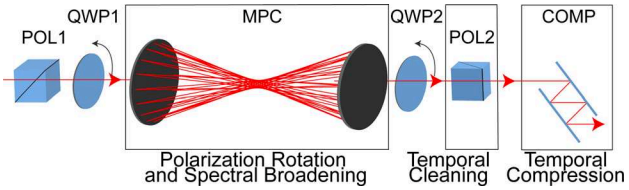

Fig. 1. Schematic setup for combined NER and post-compression using an MPC (beam incident from the left). The MPC is placed in-between crossed polarizers POL1 and POL2 and crossed quarter-wave plates QWP1 and QWP2, followed by a compressor used for chirp compensation (COMP).

show how the compressed output pulse can be optimized through polarization state control, at the expense of efficiency. Finally, we demonstrate this new regime using pulse shape measurements through frequency-resolved optical gating (FROG).

A schematic setup for implementing NER in an MPC for combined temporal contrast improvement and compression is shown in Fig. 1. The nonlinearity is introduced in the MPC through a Kerr medium; in this case, a gas or solid medium. The MPC is between two quarter-wave plates QWP1 and QWP2, oriented at angles ϕ_1 and $\phi_2 = \phi_1 + 90°$. QWP1, MPC, and QWP2 are all in-between crossed polarizers POL1 and POL2. Depending on its angle, QWP1 can convert the linear input polarization into elliptical polarization. The two orthogonal polarization components E_x and E_y, commonly illustrated together as a polarization ellipse, then accumulate different amounts of nonlinear phase, resulting in the rotation of the said ellipse [20]. For NER, these two angles are typically adjusted aiming at the highest efficiency. QWP2—typically set perpendicular to QWP1—converts the rotated and non-rotated signals into horizontal and vertical polarization. Temporal cleaning happens at the polarizer POL2, wherein the rotated parts of the pulse (now polarized perpendicular to the initial orientation) are separated from the non-rotated parts. When no nonlinearity is introduced, no rotation occurs and no signal is expected to pass POL2. Finally, a compressor is used to compensate the chirp introduced by the Kerr nonlinearity and optical elements. Both polarization rotation and spectral broadening happen in the MPC, via the optical Kerr effect. NER suppresses the pre-/post-pulses present in the input pulse, but the pre-/post-pulses that are generated after a large amount of spectral broadening appear only after the compression step. The nonlinear polarization rotation happens inside the MPC, and interchanging the positions of POL2 and COMP will not prevent the new unwanted peaks from appearing as both involve only linear processes. We assume the MPC is operating near zero dispersion, such that the spectrum is not made significantly smoother by high dispersion [18,19].

In order to better understand the physics of NER, we set up a simple analytical expression describing the process. Since the NER process can be described fully in the temporal domain, it can be written analytically, even at large B-integrals. Hence, it is possible to easily predict the efficiency of the NER process and the expected temporal contrast improvement. In contrast, modeling the output spectrum from a post-compression process, with or without NER, requires discretization of the steps and knowledge of the exact temporal pulse shape of the input. Therefore, the pre- and post-pulses appearing after compression are more difficult to predict. Modeling the whole process requires at least two orthogonal components to represent the polarization of the beam. We assume that POL1 is oriented in such a way that the output is horizontally polarized, i.e., only E_x enters QWP1. The effect of a QWP based on its angle ϕ can be written as a Jones matrix:

$$\begin{bmatrix} E_x' \\ E_y' \end{bmatrix} = \frac{1}{\sqrt{2}} \begin{bmatrix} 1 + i\cos(2\phi) & i\sin(2\phi) \\ i\sin(2\phi) & 1 - i\cos(2\phi) \end{bmatrix} \begin{bmatrix} E_x \\ E_y \end{bmatrix}. \quad (1)$$

Meanwhile, the nonlinear phase shift due to the Kerr effect, φ^{nl}, can be written as follows [21,22]:

$$E_\pm = E_\pm \exp\left(\frac{1}{3} i\varphi^{nl}\left(A_\pm^2 + 2A_\mp^2\right)\right), \quad (2)$$

wherein the circular components are related to the linear components by $E_\pm = \frac{1}{\sqrt{2}}\left(E_x \pm iE_y\right)$. Note that A refers to the amplitude and φ to the phase of the complex electric field envelope, $E_\pm = A_\pm \exp(i\varphi_\pm)$. Using circular components is more convenient since the physical process involves the angular rotation of the electric fields. The difference in phase change for E_+ and E_- results in a polarization ellipse rotation of θ, given by the following [21]:

$$\theta = -\frac{1}{3}\varphi^{nl}\sin(2\phi). \quad (3)$$

From Eqs. (1)–(3), one can derive an equation for the efficiency of the NER process, η, as a function of φ^{nl} and the QWP angles ϕ_1 and ϕ_2, where ϕ_2 is defined as $\phi_2 = 0$ when QWP2 is oriented perpendicular to QWP1 at $\phi_1 = 0$:

$$\begin{aligned} \eta(\varphi^{nl}(t), \phi_1, \phi_2) = \frac{1}{8}\Big(&4 - 2\cos(2\phi_1 - 2\phi_2) \\ &+ 2\cos(2\phi_1 + 2\phi_2) - \cos(4\phi_2 + 2\varphi^{nl}\sin(2\phi_1)/3) \\ &- \cos\left(4\phi_1 - 2\varphi^{nl}\sin(2\phi_1)/3\right) - \cos\left(2\varphi^{nl}\sin(2\phi_1)/3\right) \\ &- \cos(4\phi_1 - 4\phi_2 - 2\varphi^{nl}\sin(2\phi_1)/3)\Big). \end{aligned} \quad (4)$$

From Eq. (4), the transmission efficiency for a laser pulse with time-dependent intensity $I(t)$ is obtained by integrating $\int I(t)\eta(t)\mathrm{d}t / \int I(t)\mathrm{d}t$ over the whole temporal range, if φ^{nl} varies in time. The contrast enhancement at any given temporal point can be calculated by $\eta(\varphi^{nl}_{\mathrm{peak}}, \phi_1, \phi_2)/\eta(\varphi^{nl}_{\mathrm{peak}}/\nu, \phi_1, \phi_2)$, where ν is the initial contrast, measured as the intensity at that point divided by the peak intensity, and $\varphi^{nl}_{\mathrm{peak}}$ is the nonlinear phase shift at the peak. Note that the polarizers are assumed to be perfect, and any variation thereof would affect the contrast enhancement value.

In order to address the key challenge of temporal quality degradation in post-compression, we carried out an experiment using a laser system used for free-electron laser (FEL) pump–probe experiments at the FLASH PG Beamline, described by Seidel *et al.* in [14]. An input pulse with a duration of 1 ps at 1030 nm and 115 μJ energy is sent through an MPC with three 1-mm fused silica plates separated by 30 mm and cavity mirrors that compensate for the material dispersion of these plates. The beam inside the MPC takes 31 round trips, before being coupled out toward a grating compressor stage. The MPC in this laser system has a maximum B-integral of about 30 rad. To evaluate efficiency, we used motorized rotary mounts (Standa 8MPR16-1) for the QWPs, which allow reproducible alignment of the wave plates. We then scanned the combinations of angles as shown in Fig. 2, in steps of 1°. By the definition of ϕ_2, QWP1 and QWP2 are perpendicular along the diagonal. Indeed, our analytical expression accurately predicts the time-averaged measured efficiency. Figure 2(b) was calculated assuming that the input is

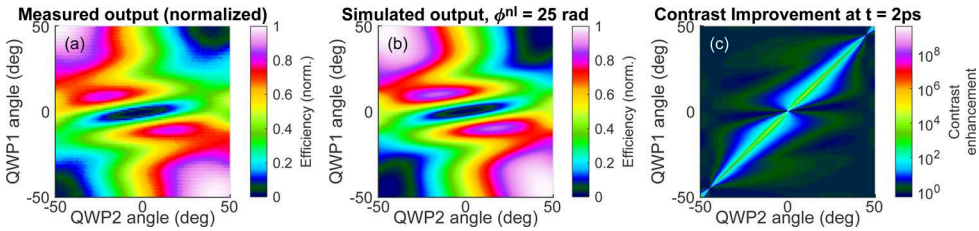

Fig. 2. NER efficiency as a function of the QWP angles, as (a) measured and (b) calculated. QWP1 and QWP2 are perpendicular along the diagonal. The simulated contrast improvement, in log-scale, is shown in (c). See Visualization 1 for different φ^{nl} values.

Gaussian-shaped. As the input pulse is a perfect Gaussian shape, without pre- and post-pulses, the contrast improvement shown in Fig. 2(c) is simply calculated at an example point t = 2 ps after the main pulse, which for a 1-ps FWHM pulse has an initial contrast $\nu_{\mathbf{input}} = \exp(-16\log(2)) \approx 1.5 \times 10^{-5}$. Along the diagonal where the QWPs are orthogonal, the contrast improvement $\nu_{\mathbf{output}}/\nu_{\mathbf{input}}$ is consistently high, with improvement values consistently above five orders of magnitude. It is worth noting that a small deviation from this diagonal could easily deteriorate the contrast by a few orders of magnitude. The contrast improvement is of course limited too by the extinction ratio of the polarizer used. This highlights the need for an accurate angle placement, as it could also be the case that the wrong angles could give higher throughput while severely losing potential contrast improvement.

The simulation in Fig. 2 does not show the effects of the pre- and post-pulses emerging in close proximity to the main pulse upon compression. To visualize this effect, we simulate the compression process using a 1D + 1 model including self-phase modulation and self-steepening, similar to what is described in [23], applied individually for each of the circular components. The spectral broadening process is highly dependent on the initial pulse shape, and since we are only assuming a perfect Gaussian shape, significant differences from experimental data are expected. The results, confined to the case where the QWPs are orthogonal to get the best contrast enhancement, are shown in Fig. 3, visualizing how both the temporal and spectral shapes vary significantly at different QWP angles. The maximum efficiency, indicated by P_1, is 70.0%. The behavior can be understood by looking at what the output pulse is composed of after POL2 analytically. After spectral broadening and nonlinear rotation, the two components $E_{\pm}$ are recombined by QWP2. The polarizer POL2 transmits only the vertical component, which can be derived using Eqs. (1) and (2) as follows:

$$|E_y|^2 = \frac{1}{2}\Big[A_+^2 + A_-^2 - 2A_+A_-\cos(2\phi + \varphi_- - \varphi_+) \times \cos(2\phi) + (A_-^2 - A_+^2)\sin(2\phi)\Big]. \tag{5}$$

It can be seen that the output is mostly the sum of the two components, along with some modulation terms depending on the phase difference and QWP angle. Since the two components experience a different amount of nonlinear phase shift (see Eq. (2)), the two also experience a different amount of spectral broadening, and adjusting this difference by changing the QWP angle effectively "shapes" the output spectrum. The characteristics of the spectra of the two components of the output spectrum can be seen in the inset in Fig. 3(b). If coherently combined with a suitable spectral broadening factor, the spectral modulation

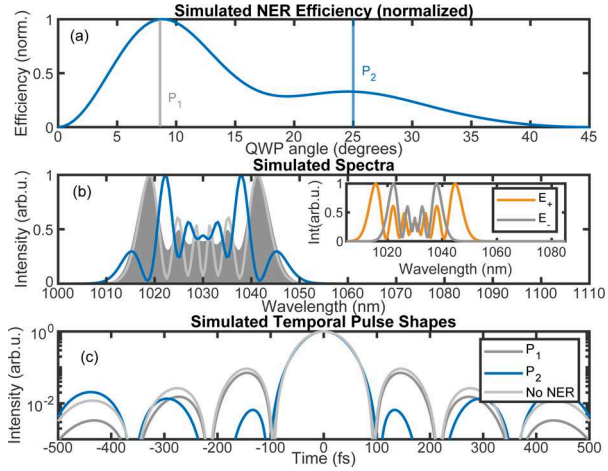

Fig. 3. (a) Normalized efficiency, (b) spectra, and (c) temporal shape of the pulse after NER and post-compression, assuming a perfect Gaussian input pulse and perfect compression (Fourier-transform-limited pulse). The inset in (b) shows the broadened spectra of the two circular components before QWP2, corresponding to the blue spectrum (P2) after passing POL2. The legend in (c) applies to the spectra in (b) as well. See Visualization 2 for different QWP angles.

reduces and a smoother spectrum is obtained at the output (blue line in Fig. 3(b)). The point P_1 in Fig. 3 represents the QWP angle at which the highest efficiency is obtained, corresponding to the set point at which NER experiments are typically set up [7,16]. Point P_2 visualizes a second example angle in comparison. By adjusting the QWP angle, it is possible to get an output pulse wherein the spectrum is shaped optimally, such that the pre- and post-pulses of the compressed pulse get weaker, specifically the strongest ones near the main pulse located at ±150 fs. This, however, comes with a drawback that the efficiency is lower.

We then verify these temporal pulse characteristics in the experiment, by measuring the temporal shapes of the compressed pulses using second-harmonic FROG. The dynamic range of the spectrometer used is 10^4, which is sufficient to measure the pre-/post-pulses near the main pulse but not the expected temporal contrast improvements at time scales much longer than the pulse duration. Note that a standard third-order cross-correlator would be difficult to use in this case due to the low energy level, but the expected contrast improvement at higher dynamic range and longer time scales have been confirmed already in [12,13]. The retrieved output spectrum shown in Fig. 4(b) can be changed significantly by changing the QWP

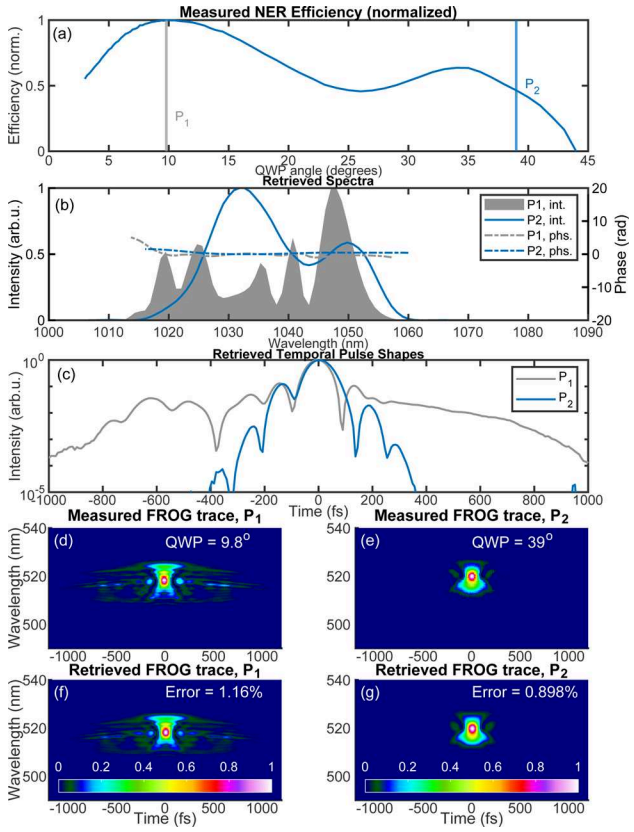

Fig. 4. (a) Normalized efficiency, (b) spectral intensity and phase, and (c) temporal shape retrieved from FROG traces. (d) FROG measurement at maximum efficiency point in P_1 and (e) at P_2 and their corresponding retrieved traces in (f) and (g). See Visualization 3 for different QWP angles.

angle, and this change can result in much improved temporal contrast of the compressed pulse. The compressed pulse measured at the highest efficiency (P_1) has the expected pre-/post-pulses near the main pulse, as also observed in the work of Pfaff *et al.*, where a high compression factor of 22 was also reached while using NER [13]. The highest efficiency obtained in the experiment is 39%. The pulse duration varies from around 70 to 90 fs (compression factors of 11–14), but note that the compressor was not optimized for each data point, although the residual phase is low as can be seen in Fig. 4(b). As the QWP angle is increased further, a much improved temporal contrast is obtained while maintaining a very similar spectral broadening and temporal compression factor. The optimum set point is clearly defined by a trade-off between contrast and efficiency, and the choice depends greatly on the desired application.

In conclusion, we have shown how NER and post-compression can be optimally combined, especially in the case of very large compression factors where the generation of new pre- and post-pulses is expected. We were able to analytically describe and experimentally demonstrate advanced polarization control in NER, enabling to get a compressed pulse with better temporal contrast. However, optimal contrast is not reached at the settings supporting the highest efficiency. The optimal set point is then chosen as a balance between peak power and temporal contrast and depends on the planned use of the laser system. For example, at the FLASH PG Beamline where the laser is used as pump for pump–probe experiments, the better contrast is highly beneficial and the slight decrease in peak power is not a problem. A stronger pre-pulse modifies the optical dynamics otherwise. Implementation of the discussed NER pulse cleaning requires only wave plates and polarizers. Therefore, the spectral shaping effect we observed provides an easier alternative to enhanced frequency compression setups [18,19] or pulse shaping techniques [24] for improving the compressed pulse's contrast.

Funding. Helmholtz Association (IVF InternLabs-0011); BMBF: Verbundproject MEGA-EUV.

Acknowledgment. We acknowledge DESY (Hamburg, Germany), a member of the Helmholtz Association HGF, for the support and the provision of experimental facilities.

Disclosures. The authors declare no conflicts of interest.

Data availability. Data underlying the results presented in this paper are not publicly available at this time but may be obtained from the authors upon reasonable request.

REFERENCES

1. A. Cotel, A. Jullien, N. Forget, *et al.*, Appl. Phys. B **83**, 7 (2006).
2. H. C. Kapteyn, M. M. Murnane, A. Szoke, *et al.*, Opt. Lett. **16**, 490 (1991).
3. A. Lévy, T. Ceccotti, P. D'Oliveira, *et al.*, Opt. Lett. **32**, 310 (2007).
4. H. Kiriyama, T. Shimomura, H. Sasao, *et al.*, Opt. Lett. **37**, 3363 (2012).
5. A. Jullien, O. Albert, F. Burgy, *et al.*, Opt. Lett. **30**, 920 (2005).
6. K. Sala and M. Richardson, J. Appl. Phys. **49**, 2268 (1978).
7. N. Smijesh, X. Zhang, P. Fischer, *et al.*, Opt. Lett. **44**, 4028 (2019).
8. M. Hanna, F. Guichard, N. Daher, *et al.*, Laser Photonics Rev. **15**, 2100220 (2021).
9. A.-L. Viotti, M. Seidel, E. Escoto, *et al.*, Optica **9**, 197 (2022).
10. V. Pajer and M. Kalashnikov, Laser Phys. Lett. **18**, 065401 (2021).
11. J. Kaur, L. Daniault, Z. Cheng, *et al.*, J. Phys. Photonics **6**, 015001 (2024).
12. J. Song, L. Shen, J. Sun, *et al.*, High Power Laser Sci. Eng. **10**, e28 (2022).
13. Y. Pfaff, C. Forster, G. Barbiero, *et al.*, Opt. Express **30**, 10981 (2022).
14. M. Seidel, F. Pressacco, O. Akcaalan, *et al.*, Laser Photonics Rev. **16**, 2100268 (2022).
15. D. Homoelle, A. L. Gaeta, V. Yanovsky, *et al.*, Opt. Lett. **27**, 1646 (2002).
16. N. Khodakovskiy, M. Kalashnikov, V. Pajer, *et al.*, Laser Phys. Lett. **16**, 095001 (2019).
17. E. Escoto, A.-L. Viotti, S. Alisauskas, *et al.*, J. Opt. Soc. Am. B **39**, 1694 (2022).
18. M. Benner, M. Karst, C. A. Mendez, *et al.*, J. Opt. Soc. Am. B **40**, 301 (2023).
19. V. S. Staels, E. C. Jarque, D. Carlson, *et al.*, Opt. Express **31**, 18898 (2023).
20. R. W. Boyd, in *Nonlinear Optics*, 4th ed. (Academic Press, 2020).
21. N. Khodakovskiy, "Methods of ultra-fast laser contrast diagnostics and optimization," Ph.D. dissertation (Freie Universitaet, 2020).
22. P. Maker, R. Terhune, and C. Savage, Phys. Rev. Lett. **12**, 507 (1964).
23. N. Daher, F. Guichard, S. W. Jolly, *et al.*, J. Opt. Soc. Am. B **37**, 993 (2020).
24. P. Balla, H. Tünnermann, S. H. Salman, *et al.*, Nat. Photonics **17**, 187 (2023).